Journal of Catalysis 273 (2010) 236–244

Contents lists available at ScienceDirect

Journal of Catalysis

journal homepage: www.elsevier.com/locate/jcat

# Correlation between structure, acidity and catalytic performance of $WO_x/Al_2O_3$ catalysts

Xueying Chen [a,b], Guillaume Clet [b], Karine Thomas [b], Marwan Houalla [b,*]

[a] Department of Chemistry and Shanghai Key Laboratory of Molecular Catalysis and Innovative materials, Fudan University, Shanghai 200433, PR China
[b] Laboratoire Catalyse et Spectrochimie, ENSICAEN, Université de Caen, CNRS, 6 Bd. du Maréchal Juin, 14050 Caen, France

ARTICLE INFO

*Article history:*
Received 30 March 2010
Revised 25 May 2010
Accepted 27 May 2010
Available online 29 June 2010

*Keywords:*
Alumina
Tungsten oxide
Surface structure
Acidity
Infrared
CO adsorption
Lutidine adsorption
Raman
Propanol dehydration

ABSTRACT

The relationship between acidity, surface structure and catalytic activity for a series of $WO_x/Al_2O_3$ catalysts was investigated. The catalysts, containing up to 4.1 atom W/nm$^2$, were prepared by incipient wetness impregnation and studied by $N_2$ physisorption, XRD, in situ Raman and infrared spectroscopy. The W phase was essentially present as surface species. Polymeric W surface species appeared above 1.4 atom W/nm$^2$; their abundance increased with W surface density. Lutidine and CO adsorption measurements, followed by infrared spectroscopy, evidenced the presence of relatively strong Brønsted acid sites. The development of these acid sites was similar to that of the abundance of polymeric W surface species. Similar evolution with W surface density was also observed for the activity for 2-propanol dehydration, an acid-catalyzed reaction, indicating a direct relationship between the abundance of polymeric W surface species, that of relatively strong Brønsted acid sites and the catalytic activity of $WO_x/Al_2O_3$ catalysts.



## 1. Introduction

A large number of industrially important reactions are catalyzed by bifunctional metal acid catalysts [1–3]. Optimizing the catalytic performance for a given application often requires a judicious control of the metal to acid ratio. We have recently shown that using the tungstated zirconia as supports, after Ir deposition, high-performance bifunctional Ir–W catalysts for selective ring opening of methylcyclohexane can be developed [4,5]. Interestingly, a nearly identical performance was obtained when Ir was deposited on tungstated alumina [6]. This suggests that similar metal–acid balance is in play in both systems and that metal–acid balance (and not the nature of the support) is the key parameter for optimum performance. The study highlights the need for a systematic study of the development of acid sites on alumina and zirconia as a function of W surface density prior to the deposition of Ir.

Since the preliminary work of Hino and Arata [7], the $WO_x/ZrO_2$ system has been extensively studied [8–22]. Tungstated zirconia catalysts are typically prepared by impregnation of zirconium oxyhydroxide and calcination at high temperature. The characterization of this system, its acidity and the catalytic behavior, in reactions such as alkane and alkene isomerization, alcohol partial oxidation, have been widely explored.

As for the $WO_x/Al_2O_3$ system, the structure, acidity and catalytic properties of these solids have been the topic of several investigations [15,23–37]. However, few studies have attempted to quantitatively analyze W speciation and abundance of acid sites and to relate the results to catalytic activity. Macht et al. [38] have examined in detail $WO_x/Al_2O_3$ and $WO_x/ZrO_2$ systems. They found that "*temporary*" Brønsted acid sites, active for butanol dehydration, were formed on reduction of $WO_x$ precursors during reaction. Interestingly, our previous studies of tungstated zirconia [20,22] and titania systems [39,40] have indicated that isopropanol dehydration activity was directly correlated with the abundance of relatively strong Brønsted acid sites *already present prior to the reaction* and to the presence of polymeric surface species. In view of these results, it is of interest to extend the study to the corresponding alumina system.

The present study will investigate the relationship between Brønsted acidity present before reaction, catalytic activity for isopropanol dehydration and W surface species on $WO_x/Al_2O_3$ catalysts. The strength and abundance of Brønsted acid sites were monitored by adsorption of two different probe molecules 2,6-dimethyl pyridine (lutidine) and CO, followed by infrared spectroscopy. CO being a weak base allows a more "absolute" evaluation of the strength of acid sites [41–45].

* Corresponding author. Fax: +33 231452822.
*E-mail address:* marwan.houalla@ensicaen.fr (M. Houalla).

0021-9517/$ - see front matter © 2010 Elsevier Inc. All rights reserved.
doi:10.1016/j.jcat.2010.05.018

In the present paper, we report a systematic study of a series of $WO_x/Al_2O_3$ catalysts with different W surface densities. A detailed characterization (elementary analysis, nitrogen physisorption, XRD, Raman) of their textures and structures was performed. The acidity was determined by lutidine adsorption at room-temperature and low-temperature CO adsorption followed by infrared spectroscopy. The catalytic performance of the $WO_x/Al_2O_3$ catalysts for an acid-catalyzed reaction, 2-propanol dehydration, was finally correlated with the abundance of their Brønsted acid sites and the surface structure of the $WO_x/Al_2O_3$ catalysts.

## 2. Experimental

### 2.1. Catalyst preparation

A series of $WO_x/Al_2O_3$ catalysts was prepared by incipient wetness impregnation of $\gamma$-$Al_2O_3$ (AX300, Criterion, treated at 773 K for 3 h before use, 245 $m^2\ g^{-1}$, 0.64 $cm^3\ g^{-1}$) with aqueous solution of ammonium metatungstate (Aldrich). After impregnation, the samples were dried for 16 h at 393 K and then calcined at 1023 K in air for 3 h. The catalysts thus prepared were designated as AlW*x*, where *x* refers to the W surface density in atom W/$nm^2$. AlW0 refers to the $Al_2O_3$ support impregnated with deionized water and subjected to the same treatment used to prepare $WO_x/Al_2O_3$ catalysts.

### 2.2. Characterization

The compositions of the as-prepared catalysts were determined by ICP-AES at the Service Central d'Analyse (USR-59/CNRS).

The Brunauer–Emmett–Teller surface areas ($S_{BET}$) were measured by $N_2$ physisorption at 77 K using an automatic adsorptiometer (Micromeritics ASAP 2000). Prior to the measurements, samples were degassed at 573 K for 2 h under vacuum. The $S_{BET}$ were determined from adsorption values for five relative pressures ($P/P_0$) ranging from 0.05 to 0.2 using the BET method. The pore volumes were determined from the total amount of $N_2$ adsorbed between $P/P_0 = 0.05$ and $P/P_0 = 0.98$.

The corrected surface area was calculated assuming that the surface area of the catalyst is only due to the alumina. It is obtained by determining the amount of alumina per g catalyst from chemical composition and normalizing the surface area to that amount.

The XRD patterns were collected on a Philips X'pert diffractometer (PW1750) with a Cu anode (K$\alpha$1, $\lambda = 0.15405$ nm) using a scanning rate of 0.0167°/s. The contribution of K$\alpha$2 was eliminated during the data analysis.

Raman spectroscopy was performed using a Jobin Yvon Labram 300 Raman spectrometer equipped with a confocal microscope, an Nd-YAG laser (frequency doubled, 532 nm) and a CCD detector. The samples were in powder form, and the power was about 13 mW. Generally, spectra were recorded at ambient temperature in the 30–1500 $cm^{-1}$ region. Raman spectra were also recorded with an in situ cell (Linkam CCR-1000), which allowed the control of both the temperature and the gas phase composition. In situ Raman spectra were collected after dehydration at 723 K for 2 h in 10% $O_2$/He flow (30 ml/min). Similar spectra were obtained after cooling to ambient conditions.

The Raman spectra of the dehydrated catalysts were curve-fitted in the 960–1100 $cm^{-1}$ region. Gaussian peaks were used at 1022.5 ± 0.5 and 1012.5 ± 0.5 $cm^{-1}$, keeping the FWHM nearly constant (19.2 ± 0.3 $cm^{-1}$).

Infrared spectra were recorded with a Nicolet Avatar FT-IR spectrometer equipped with a DTGS or MCT detector (resolution: 4 $cm^{-1}$, 128 scans). The DTGS and MCT detectors were used, respectively, for the lutidine adsorption experiments at room-temperature and for CO adsorption at low temperature (77 K). The samples were pressed into pellets (ca. 20 mg for a 2-$cm^2$ pellet) and activated at 723 K. All the spectra were recorded in situ, following activation and normalized, in the figures, to 20 mg of the solid.

For room-temperature lutidine adsorption experiments, the activation process was as follows. First, the samples were treated under vacuum at 723 K for 1 h. Then, 13.3 kPa of $O_2$ was introduced into the cell, and the samples were treated in $O_2$ at 723 K for 1 h. Finally, the samples were evacuated under vacuum for another 1 h at 723 K. After activation, the samples were cooled down to room-temperature (298 K). The infrared spectra were acquired after introduction of small increments (1.65 $cm^3$) of lutidine (2,6-dimethylpyridine) with increasing pressure into the cell. The samples were finally exposed to 133-Pa equilibrium pressure of lutidine. Thereafter, the infrared spectra were recorded following desorption at various temperatures from 323 to 573 K. These spectra were curve-fitted in the 1680–1560 $cm^{-1}$ region using six Gaussian bands located at ca. 1643, 1628, 1618, 1605, 1582 and 1572 $cm^{-1}$. The bands at ca. 1643, 1628 and 1618 $cm^{-1}$ only were used for quantification. Their FWHM were kept constant and, respectively, equal to 16, 13 and 11. The abundance of Brønsted acid sites titrated by lutidine was estimated using an integrated molar absorption coefficient value of 6.8 cm $\mu mol^{-1}$ for the sum of the ($\nu_{8a} + \nu_{8b}$) vibrations of protonated lutidine ($DMPH^+$) at ca. 1643 and 1628 $cm^{-1}$ [46]. The abundance of Lewis acid sites was calculated using the vibration of coordinated lutidine (DMPL) at ca. 1618 $cm^{-1}$ and an integrated molar absorption coefficient value of 4.4 cm $\mu mol^{-1}$ [46].

For the low-temperature CO adsorption studies, the samples, pressed as pellets, were activated in situ in the infrared cell under flowing dry air of 50 ml/min at 723 K for 2 h. The pellet was, then, cooled down in $N_2$ flow (50 ml/min) to 573 K, and the cell was evacuated for 1 h and cooled to 77 K. The infrared spectra were acquired following introduction of small doses of CO (2.15 $cm^3$) with increasing pressure and finally in the presence of 133 Pa of CO at equilibrium. These latter spectra were curve-fitted with Gaussian bands between 2140 and 2215 $cm^{-1}$. The bands were identified either directly from the spectra following introduction of small CO increments or by subtracting two spectra obtained after consecutive CO increments. For each solid, the spectra were first curve-fitted before the intense bands due to physisorbed CO were detected and after introduction of 133 Pa at equilibrium (i.e., saturation of all the acid sites). Two bands at 2172 $cm^{-1}$ (fixed) and at 2155–2162 $cm^{-1}$ were attributed to Brønsted acid sites; the bands at 2197–2212, 2189–2202 and 2177–2189 $cm^{-1}$ were ascribed to Lewis acid sites. The spectra following introduction of large doses of CO evidenced the appearance of a strong band at 2141–2143 $cm^{-1}$ and a shoulder at 2130–2132 $cm^{-1}$ characteristic of physisorbed species. For curve-fittings, FWHM of each band was kept constant. For quantification, the bands at 2172 and 2155–2162 $cm^{-1}$ were used, respectively, for monitoring relatively strong and weak Brønsted acid sites. The sum of the three bands between 2200 and 2180 $cm^{-1}$ was used for the quantification of Lewis acid sites.

### 2.3. Activity test and product analysis

2-Propanol dehydration was carried out in a fixed-bed flow reactor. The catalyst was mixed with $\alpha$-$Al_2O_3$ that was proved to be inactive for this reaction. In a typical reaction, 20 mg of catalyst mixed with 80 mg $\alpha$-$Al_2O_3$ was pretreated at 723 K in air for 2 h (ramp 5 K $min^{-1}$; 60 mL $min^{-1}$). The reaction was performed at atmospheric pressure with $N_2$ as carrier gas ($P_{2\text{-propanol}} = 1.55$ kPa) at 403 and 413 K. Reactants and products were analyzed with an online gas chromatograph (GC) (Varian CP-3380) equipped with

a capillary column (CP WAX 52 CB) and a flame ionization detector (FID).

## 3. Results and discussion

### 3.1. Catalyst texture

The BET surface area, corrected surface area of the $Al_2O_3$ support (assuming that the surface area is only due to the alumina support), W loading (determined by ICP) and the corresponding W surface density (atom W/nm$^2$) over the $WO_x/Al_2O_3$ catalysts are listed in Table 1. The W surface density of the supported $WO_x/Al_2O_3$ catalysts was estimated from the corrected surface area of the $\gamma$-$Al_2O_3$ support (see experimental section for details). As shown in Table 1, this area remains essentially constant.

### 3.2. Catalyst structure

The XRD patterns of the series of $WO_x/Al_2O_3$ catalysts for various W surface densities and for the alumina support are shown in Fig. 1. It can be clearly seen that for catalysts containing up to 3.4 atom W/nm$^2$, only the diffraction lines characteristic of $Al_2O_3$ ($2\theta$ = 37.4, 46.0 and 67.0°) are detected. This is consistent with the presence of a surface W phase in these catalysts. For W surface density of 4.1 atom W/nm$^2$, a very broad peak at $2\theta$ = 23.6° was detected indicating incipient $WO_3$ formation. A hint for the presence of this peak can also be found in the XRD pattern of the solid AlW3.8.

The Raman spectra for $WO_x/Al_2O_3$ catalysts are shown in Fig. 2. Under ambient conditions, evidences for a minor formation of $WO_3$ (Fig. 2a: bands at 805, 715 and 270 cm$^{-1}$) were found for a W surface density of 3.8 and 4.1 atom W/nm$^2$. This is consistent with XRD results. It must be noted, however, that taking into consideration the high Raman scattering cross sections of crystalline $WO_3$ when compared to that of the surface phase (two orders of magnitude according to Chan et al. [47]), the amount of $WO_3$ detected in these catalysts must be very low.

The spectra of *in situ* calcined tungstated catalysts (Fig. 2b) showed the bands characteristic of the dehydrated surface $WO_x$ species. The Raman bands at 1012–1022 cm$^{-1}$ region were attributed to the symmetric stretching vibrations of the terminal W=O bonds of surface $WO_x$ species [14,48]. A progressive shift of the position of this band from 1012 cm$^{-1}$ for AlW1.0 to 1022 cm$^{-1}$ for AlW3.8 and AlW4.1 is observed. This was ascribed to an increased degree of polymerization of W species with increasing W surface density [12,14,15,20].

To assess the evolution of the abundance of the polymeric W surface species, the Raman spectra of the dehydrated catalysts were curve-fitted in the 960–1100 cm$^{-1}$ region. Decomposition of the envelope characteristic of $\nu$(W=O) vibration indicates the presence of two bands at ca. 1022 and 1012 cm$^{-1}$. Based on previous results [20,22], these bands were ascribed to the presence of two types of W surface species with different degrees of condensation (respectively polymeric W and either monomeric or in a low-condensed form of W species). Similar behavior has also been shown for the $NbO_x/ZrO_2$ [49] and $NbO_x/TiO_2$ [50] systems. Fig. 3 shows the evolution of the abundance of polymeric W surface species

**Table 1**
Physicochemical properties of $WO_x/Al_2O_3$ catalysts.

| Sample | W loading (wt.%) | $S_{BET}$ ($m^2\,g^{-1}$) | $S_{corrected}$ ($m^2\,g^{-1}$) | W surface density (atom W/nm$^2$) |
|---|---|---|---|---|
| AlW0 | – | 217.2 | – | – |
| AlW1.0 | 6.64 | 223.2 | 243.6 | 0.96 |
| AlW1.4 | 9.24 | 216.0 | 244.5 | 1.36 |
| AlW2.0 | 13.05 | 208.1 | 249.1 | 1.97 |
| AlW3.1 | 19.00 | 190.8 | 250.9 | 3.06 |
| AlW3.4 | 20.48 | 182.5 | 246.0 | 3.43 |
| AlW3.8 | 22.24 | 175.8 | 244.3 | 3.84 |
| AlW4.1 | 23.17 | 169.2 | 239.0 | 4.13 |

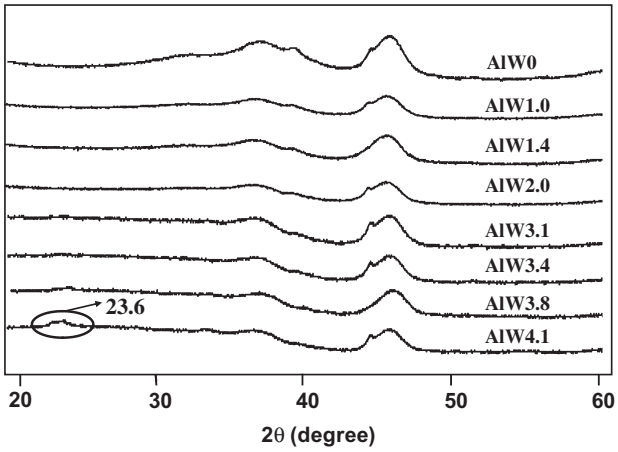


**Fig. 1.** XRD patterns for the series of $WO_x/Al_2O_3$ catalysts.

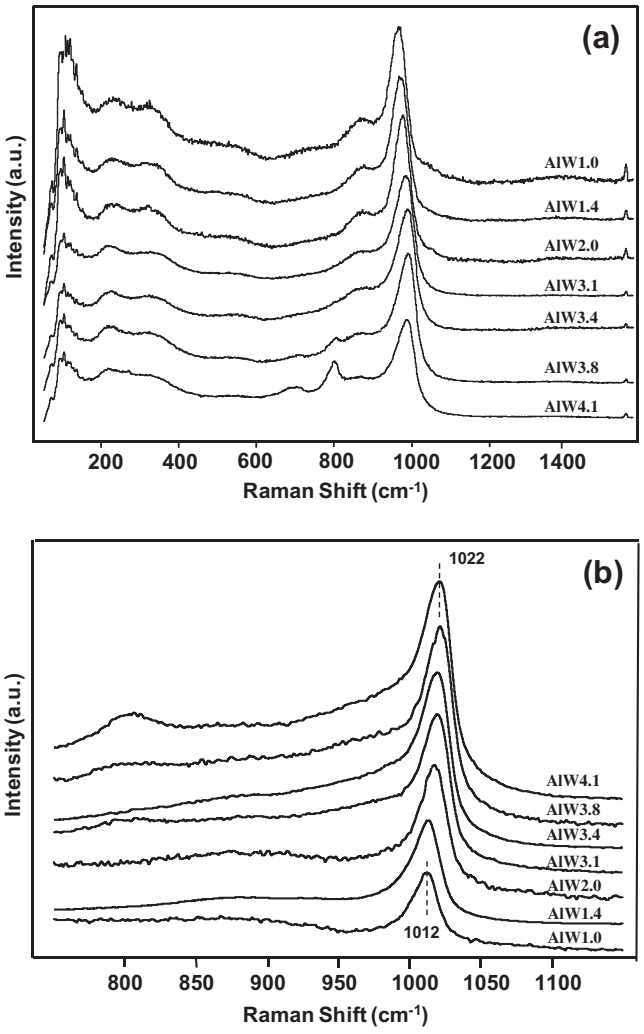


**Fig. 2.** Raman spectra for the series of $WO_x/Al_2O_3$ catalysts at ambient (a) and dehydrated (b) conditions.

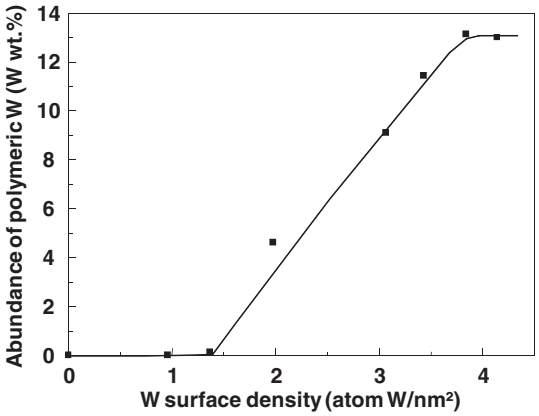


**Fig. 3.** Evolution of the abundance of polymeric W surface species as a function of W surface density of $WO_x/Al_2O_3$ catalysts. (Abundance of polymeric W surface species is defined as the fraction of polymeric W multiplied by the W loading.)

(fraction of polymeric W × W loading) as a function of W surface density. The fraction of polymeric W surface species was calculated from the area ratio of the curve-fitted band at ca. 1022 $cm^{-1}$ and the whole envelope (Fraction = $A_{1022}/A_{envelope}$). This calculation should be considered as a first approximation since it implies that both polymeric and monomeric W species exhibit similar Raman scattering cross sections. However, calculations carried out by assuming different cross sections for both species yielded similar trend.

The results show that for W surface density $\leqslant$1.4 atom W/$nm^2$, the abundance of polymeric W surface species was very low or negligible. Significant formation of polymeric W surface species was observed for a W surface density of 2.0 atom W/$nm^2$, followed by a steady increase in their abundance with increasing W surface density up to 3.8 atom W/$nm^2$ and leveling off above. This is consistent with UV–Vis spectroscopy results reported by Ross-Medgaarden and Wachs [51] which indicate the presence of monomeric W species or a mixture of monomeric and polymeric species in $WO_x$/alumina catalysts containing, respectively, 0.5 and 4.5 atom W/$nm^2$.

### 3.3. Catalytic dehydration of 2-propanol

2-propanol dehydration is a well-established probe reaction for monitoring the acidity of solid acids [52]. Under our experimental conditions, the $\gamma$-$Al_2O_3$ support was not active. Over $WO_x/Al_2O_3$ catalysts, propene and diisopropyl ether were the only products observed. The selectivity to propene was generally higher than 80%.

The propene formation rate at 403 K and the TOF values (defined as propene formation rate per W atom) over the $WO_x/Al_2O_3$ catalysts are plotted in Fig. 4 as a function of W surface density. Similar trend was observed at 413 and 423 K. It can be clearly seen that a minimum of W surface density is required for the development of the activity. Catalysts containing W surface densities $\leqslant$1.4 atom W/$nm^2$ exhibit little or no activity. For W surface density >1.4 atom W/$nm^2$, the propene formation rate drastically increased with increasing W surface densities up to 4.1 atom W/$nm^2$ (Fig. 4a). Similar evolution was observed for the TOF (Fig. 4b). The observed behavior can be explained as follows: For low W surface densities, $WO_x$ species are essentially in a monomeric (or a low degree of condensation) form, which is considered to be less susceptible of generating relatively strong Brønsted acid sites and thus less active [22]. The observed increase in the TOF with increasing W surface density can be attributed to an increased formation of polymeric $WO_x$ species, which are, reportedly, associated with the development of Brønsted acidity and activity in the case of tungstated zirconia [22].

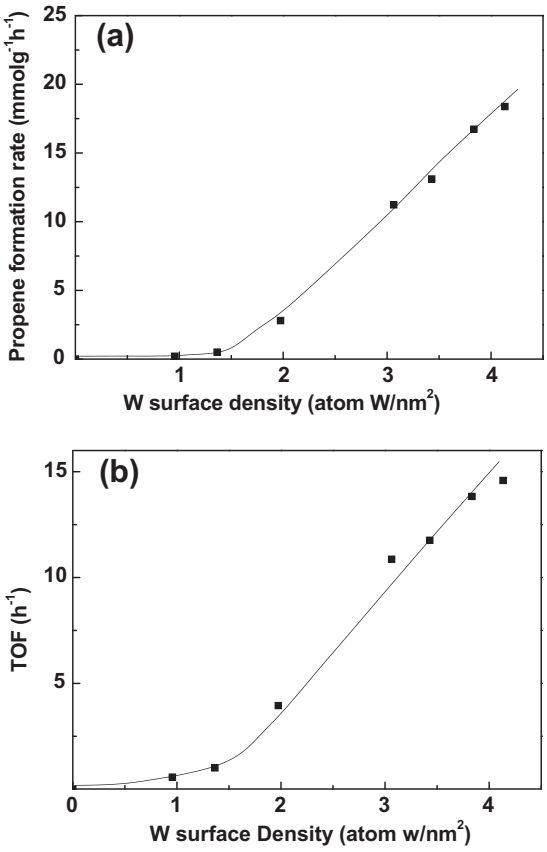


**Fig. 4.** Propene formation rate (a) and TOF (b) as a function of W surface density of $WO_x/Al_2O_3$ catalysts at a reaction temperature of 403 K.

### 3.4. Acidity

#### 3.4.1. Lutidine adsorption

Several probe molecules including carbon monoxide, pyridine and lutidine can be used to characterize the acidity of oxide surfaces. Lutidine was preferred over pyridine in the present study because it is a more sensitive probe of Brønsted acid sites due to its higher basicity [53,54]. Fig. 5 displays the infrared spectra of catalysts (after subtraction of the spectrum of the activated catalysts) following equilibrium adsorption of 133 Pa of lutidine and desorption under vacuum at 573 K. For comparison, the infrared spectrum for the AlW0 support is also shown.

The infrared spectrum for lutidine adsorption over the AlW0 support, following desorption at 573 K, exhibits two main bands at ca. 1618 and 1583 $cm^{-1}$, attributed to $\nu_{8a}$ and $\nu_{8b}$ vibrations of lutidine coordinated to the Lewis acid sites [55]. In addition, a weak shoulder is observed at 1653 $cm^{-1}$, which is attributed to $\nu_{8a}$ vibration of lutidine protonated on weak Brønsted acid sites of the $Al_2O_3$ [56]. The position of the shoulder appears to shift to lower wavenumbers with increasing W surface density (from 1645 $cm^{-1}$ for AlW1.0 and AlW1.4 solids to 1640 $cm^{-1}$ for AlW3.8 and AlW4.1). The shift was accompanied with a drastic increase in intensity of the corresponding band. The $\nu_{8a}$ band of lutidine is reportedly sensitive to the strength of the Brønsted acid sites [56]. Thus, it is reasonable to assume that the strength of the Brønsted acidity increased with increasing W surface density.

To assess the evolution of the abundance of Brønsted and Lewis acid sites with W surface density, the spectra of the catalysts were

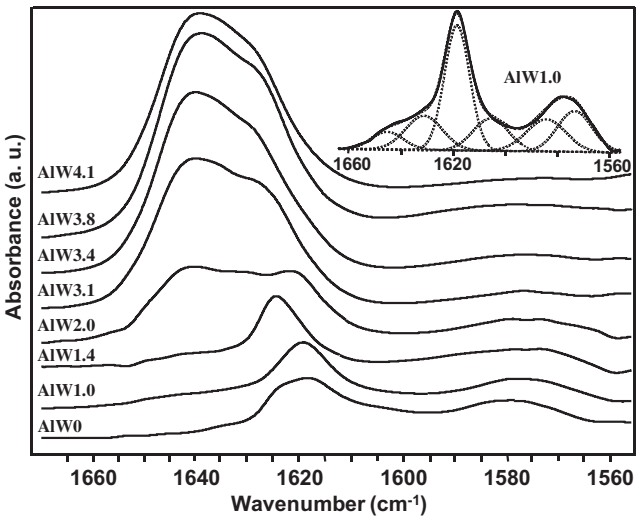


**Fig. 5.** Infrared spectra for the series of $WO_x/Al_2O_3$ catalysts after saturation of the surface with 133-Pa lutidine and desorption under vacuum at 573 K and following subtraction of the spectrum of the activated catalysts. The inset shows typical curve-fitting results (AlW1.0 was used as an example. Solid line: experimental spectrum; Dotted line: individual peaks after curve-fitting).

curve-fitted in the 1680–1560 $cm^{-1}$ region using six Gaussian bands located at ca. 1643, 1628, 1618, 1605, 1582 and 1572 $cm^{-1}$ as depicted in the inset in Fig. 5. These bands are ascribed to the $\nu_{8a}$ and $\nu_{8b}$ vibrations of lutidine bound to Brønsted acid sites (1643 and 1628 $cm^{-1}$), Lewis acid sites (1618 and 1582 (or 1572) $cm^{-1}$) and H-bound lutidine (1605 and 1572 (or 1582) $cm^{-1}$) [46,55,56]. Fig. 6 shows the evolution of the abundance of Brønsted (sum of the bands at ca. 1643 and 1628 $cm^{-1}$) and Lewis (band at ca. 1618 $cm^{-1}$) acid sites after lutidine desorption at 573 K for the series of $WO_x/Al_2O_3$ catalysts with different W surface densities. The results clearly show that the abundance of Brønsted acid sites was negligible for the alumina support and low for W surface density $\leqslant$1.4 atom W/$nm^2$. For higher W surface densities, a significant and a steady increase in the abundance of Brønsted acid sites was observed until 3.8 atom W/$nm^2$. This increase appears to level off for higher W surface density. The abundance of Lewis acid sites determined from the intensity of the band at 1618 $cm^{-1}$ (Fig. 6b) decreased with increasing W surface density. This can be ascribed to an increased coverage of the alumina support on W deposition [27].

It must be noted, however, that the abundance of Brønsted acid sites obtained following lutidine desorption at 573 K only reflects the number of Brønsted acid sites that are able to retain lutidine after such treatment. Thus, it cannot be considered as a measure of a specific acid strength. In order to gain additional insight into the strength of Brønsted acid sites, low-temperature CO adsorption studies were performed.

### 3.4.2. Low-temperature CO adsorption

CO is an efficient probe molecule for the evaluation of the acid strength of the Brønsted sites. At low temperature (77 K), it can form coordination bonds with Lewis acid sites and hydrogen bonds with Brønsted acid sites with ensuing perturbation of the vibration of surface hydroxyl group. The formation of the OH···CO complexes gives rise to a downward frequency shift of the O—H stretching mode and simultaneously an upward shift of the C—O stretching mode when compared to that recorded in the gas phase at ca. 2143 $cm^{-1}$. The extent of the shift provides useful information on the strength of the Brønsted acid sites of the solids [44,45].

After activation at 723 K, the most noticeable changes in the infrared spectra of different catalysts were observed in the OH region (Fig. 7). For the alumina support (AlW0), five main $\nu$(OH) bands at ca. 3795, 3775, 3762, 3734 and 3680 $cm^{-1}$ are observed, in agreement with the results of Knözinger and Ratnasamy [57]. On W deposition, the intensity of the area associated with the OH stretching region decreased gradually with increasing W surface density. This can be ascribed to the progressive replacement of the OH groups by the W species, as it has been observed for several metal oxides supported on alumina [58,59] or zirconia [60]. For W surface density $\geqslant$2.0 atom W/$nm^2$, the various $\nu$ (OH) frequencies that were easily resolved for $Al_2O_3$ become ill-defined.

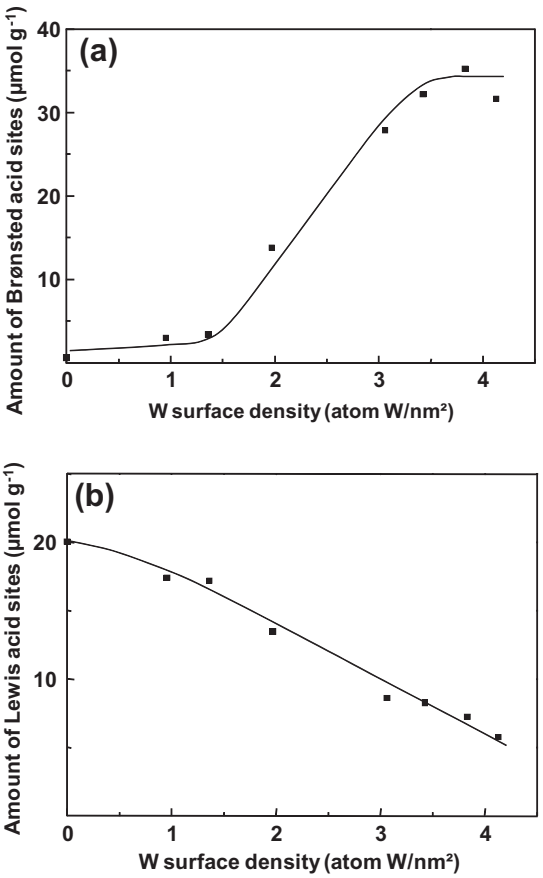


**Fig. 6.** Evolution of the abundance of Brønsted (a) and Lewis acid sites (b) following lutidine desorption at 573 K for the $WO_x/Al_2O_3$ catalysts.

Infrared spectra for representative solids were obtained following addition of small increments of CO. This approach permits the detection of the strongest acid sites since these sites will react first. It has also the added advantage of acquiring the spectra under conditions that minimize CO physisorption, thus facilitating curve-fitting. Fig. 8 shows the infrared spectra for representative solids following the introduction of a small dose of CO (2.3 μmol). Two bands are observed: a broad band above 2180 $cm^{-1}$ characteristic of Lewis acid sites and a band at 2166–2173 $cm^{-1}$ characteristic of the strongest Bronsted acid sites. For W surface density $\geqslant$2.0 atom W/$nm^2$, the band is centered at ca. 2172 $cm^{-1}$. The emergence of this band coincides with the development in the hydroxyls region, of a prominent band at ca. 3455 $cm^{-1}$ which corresponds to $\Delta\nu$(OH) shift, for the hydroxyls perturbed by the interaction with the CO molecule, of 252 $cm^{-1}$. The magnitude of this shift is indicative of the presence of relatively strong Brønsted acid sites [44]. One can also estimate from the correlation reported by Cairon et al. [44], between $\Delta\nu$(OH) of the hydroxyls perturbed by the interaction with the CO molecule and the position of the corresponding $\nu$(CO) stretching vibration, that such a shift is associated

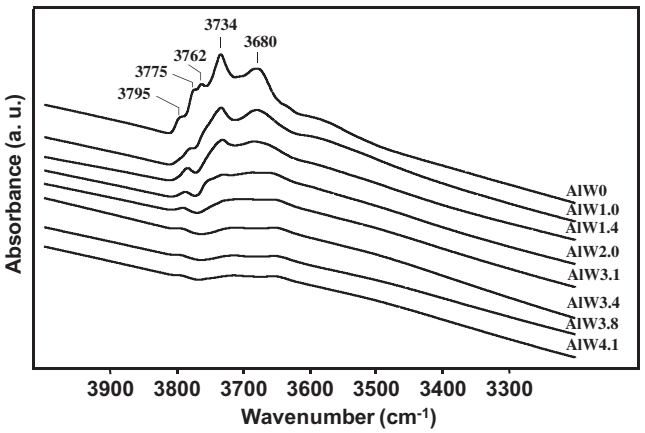


**Fig. 7.** Infrared spectra of the $\nu$(OH) region for the AlW0 support and the series of $WO_x/Al_2O_3$ catalysts after activation at 723 K.

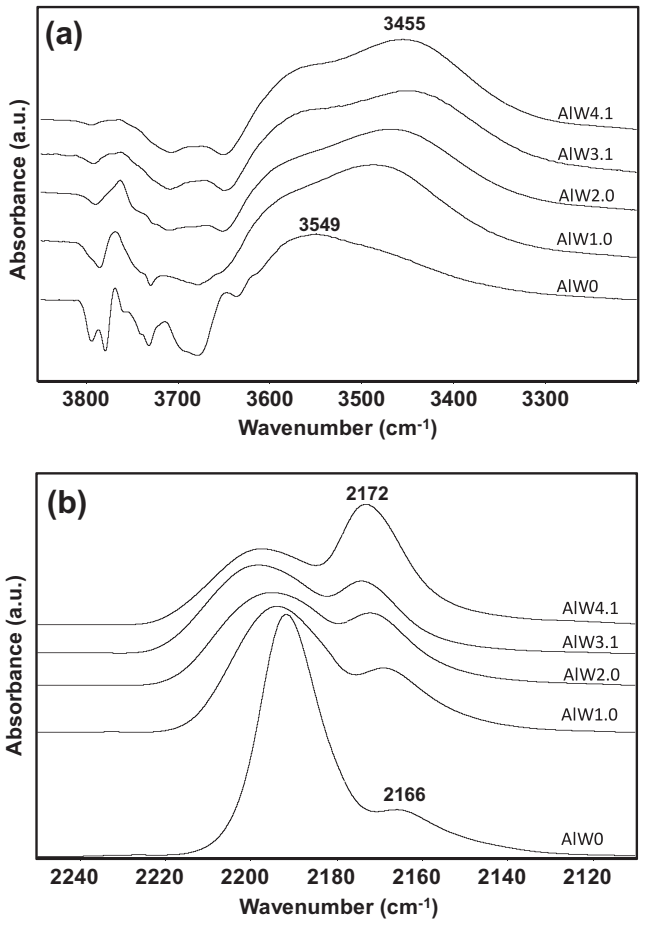


**Fig. 8.** Infrared spectra for the series of $WO_x/Al_2O_3$ catalysts after introduction of 2.3 μmol CO and subtraction of the spectrum of the activated catalyst. (a) $\nu$(OH) region, (b) $\nu$(CO) region.

with $\nu$(CO) stretching vibration at 2171 $cm^{-1}$. This confirms that the band at 2172 $cm^{-1}$ originates from CO interaction with the above-mentioned Brønsted acid sites. With increasing amounts of CO introduced, the average position of the $\nu$(CO) progressively shifted to lower wavenumbers as larger amounts of weaker sites were detected. The band at 2172 $cm^{-1}$ becomes progressively hidden by that of CO adsorbed on weaker acid sites.

Fig. 9a presents the infrared spectra in the $\nu$ (OH) region obtained after equilibrium adsorption of 133-Pa CO and subtraction of the spectrum of the activated catalysts. For the AlW0 support, the band at 3734 $cm^{-1}$ was shifted to ca. 3616 $cm^{-1}$ ($\Delta\nu$(OH) = 118 $cm^{-1}$). For low W surface density ($\leqslant$1.4 atom W/$nm^2$) catalysts, only this hydroxyl group seems to be perturbed by CO but the $\Delta\nu$(OH) shift increased gradually with W surface density indicating an increase in the strength of the Brønsted acid sites present in AlW0, AlW1.0 and AlW1.4. With further increase in the W surface density ($\geqslant$2.0 atom W/$nm^2$), in addition to the previous OH perturbation at 3734 $cm^{-1}$, another OH band at ca. 3707 $cm^{-1}$ was perturbed and shifted to lower wavenumbers. The band, broad and ill-defined, is centered around 3515–3460 $cm^{-1}$ ($\Delta\nu$(OH) ~ 192–247 $cm^{-1}$) indicating the presence of Brønsted acid sites that are significantly stronger than those observed for lower W surface density.

In the $\nu$(CO) region (Fig. 9b), for the alumina support, CO adsorption at 77 K gives rise to a strong band at 2155 $cm^{-1}$ and a shoulder at 2143 $cm^{-1}$. As reported in the literature [43], the band at ca. 2155 $cm^{-1}$ can been assigned to CO hydrogen weakly bonded to OH groups on the alumina support, whereas that at ca. 2141–2144 $cm^{-1}$ (a frequency very close to that of the free CO molecule) can be ascribed to CO physisorbed on the alumina surface. A broad

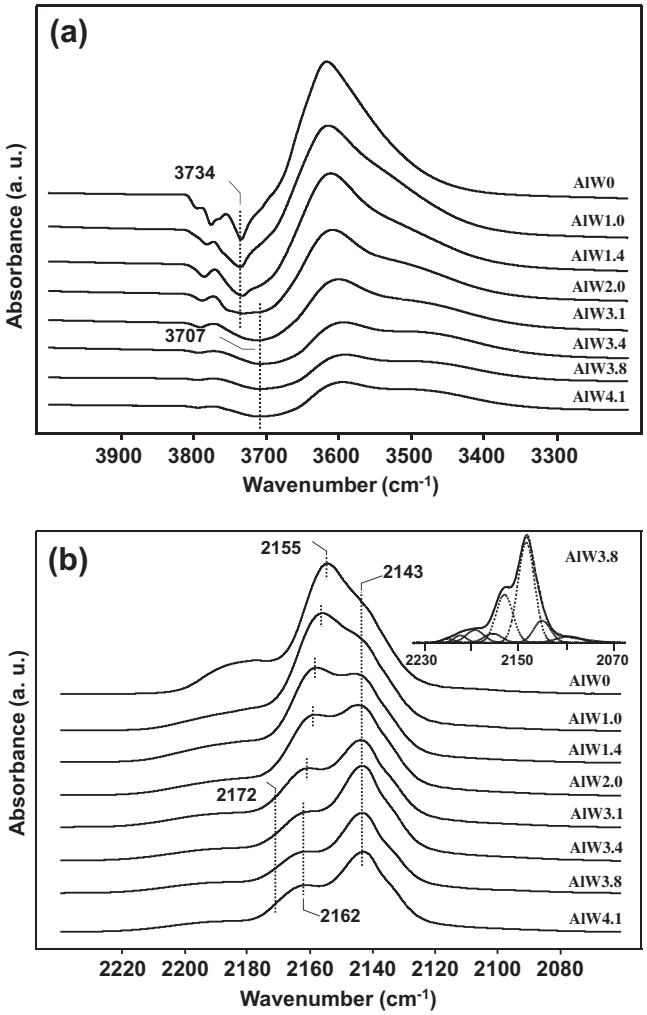


**Fig. 9.** Infrared spectra for the series of $WO_x/Al_2O_3$ catalysts after introduction of 133-Pa CO at equilibrium and subtraction of the spectrum of the activated catalyst. (a) $\nu$(OH) region, (b) $\nu$(CO) region. The inset in Fig. 8b shows typical curve-fitting results (AlW3.8 was used as an example. Solid line: experimental spectrum; Dotted line: individual peaks after curve-fitting).

shoulder, in the 2215–2180 $cm^{-1}$ region, attributed to CO coordinated to $Al^{3+}$ sites [45,61], is also observed. For $WO_x/Al_2O_3$ solids, the $\nu$(CO) frequency is shifted upward from 2155 $cm^{-1}$ for the alumina support to 2160 $cm^{-1}$ for AlW3.1. This was accompanied with a strong decrease in intensity. This upward shift of the $\nu$(CO) frequency at 2155 $cm^{-1}$ is consistent with the reported preferential consumption of the most basic OH groups on initial W deposition in the case of $WO_x/ZrO_2$ or with initial addition of Mo for the related $MoO_x/Al_2O_3$ system [60,62]. With further increases in the W surface density to 3.1 atom W/$nm^2$ and higher, the $\nu$(CO) band shifted to 2162 $cm^{-1}$. Simultaneously, a new band at higher frequency appears to develop.

To monitor the evolution of the abundance of Brønsted and Lewis acid sites with W surface density following equilibrium adsorption, the infrared spectra of the catalysts after 133-Pa adsorption of CO at equilibrium were thus curve-fitted in the 2240–2140 $cm^{-1}$ region. As depicted in the inset in Fig. 9b, the envelope can be curve-fitted using six Gaussian bands: The three bands located at ca. 2180–2205 $cm^{-1}$ assigned to Lewis acid sites; the band at 2172 $cm^{-1}$ assigned to relatively strong Brønsted acid sites, that at 2155–2162 $cm^{-1}$ originating from weak Brønsted acid sites and the band at 2143 $cm^{-1}$ corresponding to physisorbed CO. Fig. 10 shows the evolution of the abundance of the acid sites as a function of W surface density. The abundance of weak Brønsted acid sites and Lewis acid sites decreased with increasing W surface density (Fig. 10). This can be ascribed to an increased coverage of the alumina support on W deposition [27].

In contrast, as depicted in Fig. 10a, a different evolution of relatively strong Brønsted acid sites (band at 2172 $cm^{-1}$) was observed. These acid sites were not detected for W surface density lower than 1.4 atom W/$nm^2$. For W surface density $\geqslant$2.0 atom W/$nm^2$, the abundance of these acid sites increased almost linearly with increasing W surface density.

### 3.4.3. Comparison between lutidine and CO adsorptions

Fig. 11 compares the development of Brønsted acidity as monitored by lutidine and low-temperature CO adsorption. Overall, similar evolution is observed with both probe molecules. In both instances, a minimum of W surface density appears to be required for the development of Brønsted acidity. Above this threshold, the abundance of these acid sites increased almost linearly with increasing W surface density. However, while Brønsted acid sites titrated by lutidine after desorption at 573 K were detected at a W surface density of ca. 1.0 atom W/$nm^2$, those monitored by CO adsorption (band at 2172 $cm^{-1}$) were only observed at 2.0 atom W/$nm^2$. This can be attributed to the fact that the band at 2172 $cm^{-1}$ observed for CO adsorption measurements is associated with Brønsted acid sites of a specific strength, whereas lutidine desorption measurements titrate all the Brønsted acid sites that are sufficiently strong to retain lutidine following desorption at 573 K. The latter may comprise weaker Brønsted acid sites than those monitored by low-temperature CO adsorption.

### 3.5. Correlation between Brønsted acidity and catalytic activity

Fig. 12 depicts the evolution of the propene formation rate as a function of the abundance of Brønsted acid sites determined by lutidine desorption at 573 K and low-temperature CO adsorption over the $WO_x/Al_2O_3$ catalysts. A direct relationship is clearly observed between the catalytic activity and the abundance of Brønsted acid sites present on the catalyst, prior to the reaction, monitored by both probe molecules. Similar results were previously reported by Lebarbier et al. on tungstated zirconia catalysts using lutidine desorption at 573 K [22]. However, a close inspection of the data shows that unlike the results for tungstated zirconia, the activity of $WO_x/Al_2O_3$ catalysts for low W surface density

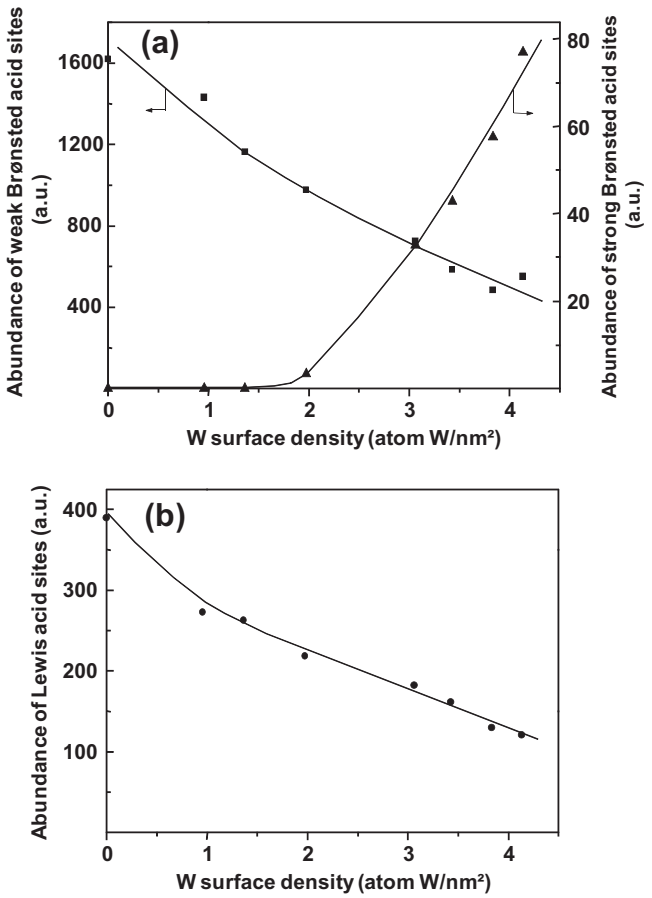


**Fig. 10.** Evolution of the abundance of acid sites for $WO_x/Al_2O_3$ catalysts after introduction of 133-Pa CO at equilibrium at 77 K. (a) strong (band at 2172 $cm^{-1}$: ▲) and weak (band at 2155–2162 $cm^{-1}$: ■) Brønsted acid sites; (b) Lewis acid sites (sum of the three bands at 2180–2200 $cm^{-1}$: ●).

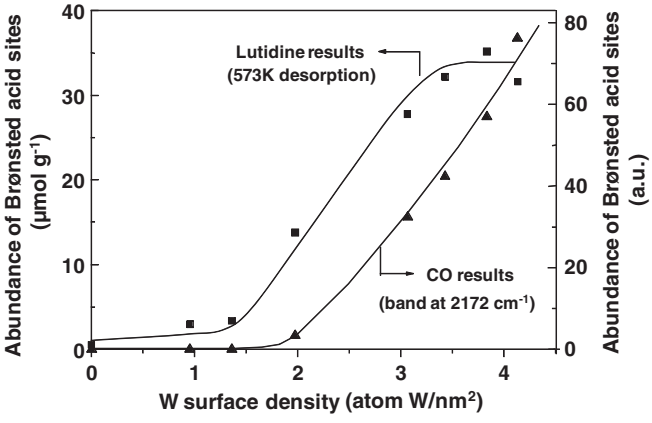


**Fig. 11.** Comparison of the abundance of Brønsted acid sites estimated from lutidine adsorption followed by desorption at 573 K (■) and low-temperature CO adsorption using the band at 2172 $cm^{-1}$ (▲).

AlW1.0 and AlW1.4 is negligible despite evidence of the presence of Brønsted acid sites. This might indicate that some of the acid sites measured by lutidine are not sufficiently strong to catalyze efficiently isopropanol dehydration. This is consistent with the high wavenumber of the $\nu_{8a}$ band observed for these solids (i.e., low strength of Brønsted acid sites) as compared to other catalysts (Section 3.4.1). In contrast, examination of CO adsorption results

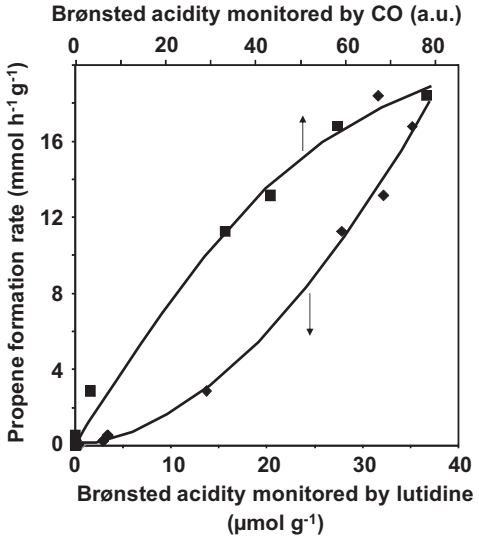


**Fig. 12.** Evolution of propene formation rate over the $WO_x/Al_2O_3$ catalysts as a function of the abundance of Brønsted acid sites estimated from lutidine adsorption followed by desorption at 573 K (♦) and from the intensity of the CO band at 2172 $cm^{-1}$ (■).

shows that propene formation activity develops before the detection of the band at 2172 $cm^{-1}$ characteristic of relatively strong Brønsted acid sites. This indicates that Brønsted acid sites monitored by the CO band at 2172 $cm^{-1}$ are stronger than those required for the onset of activity for 2-propanol dehydration.

### 3.6. Correlation between catalyst structure, Brønsted acidity and catalytic activity

Fig. 13 depicts the evolution of the abundance of polymeric W surface species, Brønsted acid sites measured by lutidine desorption at 573 K and the catalytic activity for 2-propanol dehydration as a function of the W surface density. Clearly, a similar trend is observed below the monolayer, indicating a direct relationship between polymeric W surface species, relatively strong Brønsted acidity and catalytic performance. These findings are consistent with previous results, albeit qualitative, obtained with the same catalytic system [31,32,63]. Ponec and coll. [31,32] reported for

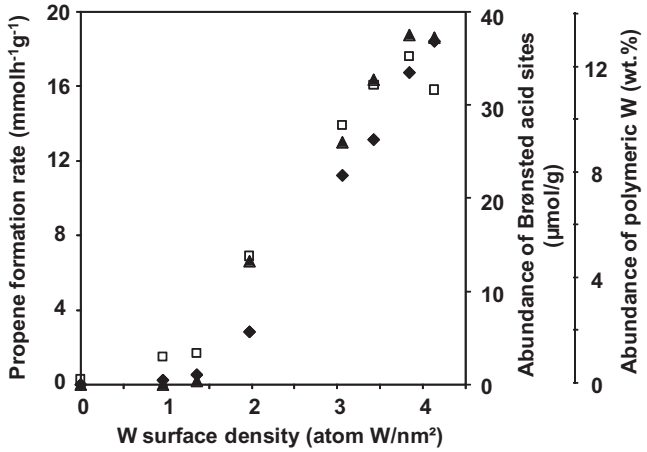


**Fig. 13.** Evolution of the propene formation rate (♦), abundance of the strong Brønsted acid sites measured by lutidine adsorption (□) and abundance of polymeric W surface species (▲) as a function of W surface density of $WO_x/Al_2O_3$ catalysts.

skeletal isomerization of 1-butene, a Brønsted acid-catalyzed reaction, an increase in conversion to isobutene with W loading. This was attributed to an increased formation of dimeric $WO_4^{2-}$ at the detriment of monomeric $WO_4^{2-}$ species and concomitant development of Brønsted acidity.

### 3.7. Comparison with others supported W systems

In our previous studies of $WO_x$/zirconia [20,22] and $WO_x$/titania [39,40,64] systems, a direct relationship between the abundance of Brønsted acid sites or polymeric W surface species and the catalytic activity for 2-propanol dehydration was established. The results presented here indicate that a similar correlation is observed in the case of $WO_x/Al_2O_3$ catalysts. For all these tungstated catalysts, a similar threshold of the W surface density of ca. 1.2–1.4 atom W/$nm^2$ was observed for the development of relatively strong Brønsted acidity and significant dehydration activity. Above this threshold and below monolayer coverage (4–5 atom W/$nm^2$ [16]), the abundance of relatively strong Brønsted acid sites, polymeric W surface species and propanol dehydration activity increased almost linearly with further increases in the W surface density. It is worth noting that these correlations were obtained for systems using as a support a crystallized oxide (tetragonal [22] or monoclinic [20] zirconia, anatase [39] or mixed anatase/rutile [40,64] for $TiO_2$) or amorphous oxyhydroxides (Zr or Ti oxyhydroxides) [22,39].

These results can be compared with previously reported findings for butanol dehydration [38]. This reaction was reported to be catalyzed by Brønsted acid sites [10,38]. Macht et al. [38] found that butanol dehydration activity on tungstated alumina and zirconia evolved in the same manner with W surface density. For both systems, a maximum in the TOF was observed for W surface densities of ca. 9–10 atom W/$nm^2$. The evolution of the activity with increasing W surface density was associated with the increase in $WO_x$ domain size. For the purpose of comparison with the present study, additional solids containing higher W surface densities (5.5 and 9.1 atom W/$nm^2$) were synthesized and tested for isopropanol decomposition under the same conditions used for solids in the submonolayer range (Fig. 4). TOF's of 14.2 and 7.9 $h^{-1}$ were, respectively, obtained vs. 14.6 $h^{-1}$ for the solid containing 4.1 atom W/$nm^2$. This indicates a maximum in the TOF for W surface densities between 4.1 and 5.5 atom W/$nm^2$. The decline in the TOF for W surface density significantly higher than those reported for monolayer coverage (4–5 atom W/$nm^2$) can be ascribed to the formation of poorly dispersed crystalline $WO_3$ evidenced by XRD and Raman Spectroscopy. Overall, the evolution of the TOF with W surface density is, thus, similar to that reported by Iglesia and coworkers [38], although the maximum in the present study was reached at a lower W surface density. This may be attributed to a more significant formation of poorly dispersed $WO_3$ in the present study above nominal monolayer coverage. The main difference between the two studies is that the activity was correlated with *temporary Brønsted acid sites formed on reduction in these WOx domains with butanol* [38]. Our results with both CO and lutidine probe molecules show that the catalytic performance can be correlated with the abundance of relatively strong Brønsted acid sites that are present *prior to the reaction* and with the abundance of W polymeric surface species.

Recently, Kim et al. have investigated the structure–surface acidity relationships for supported $WO_x$ catalysts [15]. Methanol dehydration was used as a probe reaction. Various supports were examined including alumina. The authors proposed that the influence of W surface density on the TOF depends on the relative acidity of the W surface species when compared to that of $WO_3$ nanoparticles. Their results indicate that the TOF for zirconia, titania and niobia supports increases with W surface density whereas

that of alumina-supported catalysts decreases. This was attributed to the fact that only in the latter case, the acidity of W surface species is higher than that of $WO_3$ nanoparticles. However, for the latter system, only the results obtained for W surfaces densities above monolayer coverage were reported. This was due to the high activity of exposed alumina sites in the submonolayer region when compared to that of surface tungstate species present in this region. Above monolayer coverage, their results for the $WO_x/Al_2O_3$ system indicate a decrease in the TOF with increasing W surface density, which is consistent with the results obtained in the present work. More detailed study of the zirconia-supported catalysts by the authors shows an increase in TOF with increasing W surface density in the *submonolayer region* which was attributed to a greater "catalytic acidity" of surface polytungstate species compared to surface monotungstate species. This is consistent with the results reported in the present study for alumina-supported systems.

## 4. Conclusions

The study of the structure, acidity and catalytic activity of a series of $WO_x/Al_2O_3$ catalysts prepared by incipient wetness impregnation and containing a submonolayer W coverage was performed. The results indicated the following:

A minimum of W surface density (1.4 atom W/nm$^2$) is required for the appearance of relatively strong Brønsted acid sites. For higher W surfaces densities, a steady increase in the abundance of these acid sites with W surface density was observed.

Analysis of the structures of the solids by XRD and Raman spectroscopy reveals the presence of a threshold for the formation of polymeric W species (1.4 atom W/nm$^2$) that is similar to that observed for the development of Brønsted acidity.

The abundance of relatively strong Brønsted acid sites detected before reaction and that of polymeric W surface species were found to correlate with 2-propanol dehydration activity.

The structure/acidity/activity relationship evidenced in the present study extends those previously reported for other zirconia- and titania-supported systems [20,22,39,40,49,50]. For a given support and in the submonolayer region, these relationships are indicative of a general pattern for the development of Brønsted acid sites with increasing surface density of W and other related supported phases.

## Acknowledgments

This work was supported by the Fondation Franco-Chinoise pour la Science et ses Applications (FFCSA), the NSF of China (20803009) and by Total S.A.

## References

[1] S.T. Sie, in: G. Ertl, H. Knözinger, J. Weitkamp (Eds.), Handbook of Heterogeneous Catalysis, Vol. 4, Wiley, VCH, 1997, p. 1998.
[2] I.E. Maxwell, J.K. Minderhoud, W.H.J. Stork, J.A.R. van Veen, in: G. Ertl, H. Knözinger, J. Weitkamp (Eds.), Handbook of Heterogeneous Catalysis, Vol. 4, Wiley, VCH, 1997, p. 2017.
[3] W. Vermeiren, J.P. Gilson, Top. Catal. 52 (2009) 1131.
[4] S. Lecarpentier, J. van Gestel, K. Thomas, M. Houalla, J. Catal. 245 (2007) 45.
[5] S. Lecarpentier, J. van Gestel, K. Thomas, J.-P. Gilson, M. Houalla, J. Catal. 254 (2008) 49.
[6] J.W. Park, K. Thomas, J.V. Gestel, J.-P. Gilson, C. Collet, J.-P. Dath, M. Houalla, Study of Ir/$WO_3/Al_2O_3$ selective ring opening catalysts. in: Europacat IX, Salamanca, Spain, 2009, p. 335.
[7] M. Hino, K. Arata, J. Chem. Soc. Chem. Commun. (1988) 1259.
[8] D.G. Barton, S.L. Soled, G.D. Meitzner, G.A. Fuentes, E. Iglesia, J. Catal. 181 (1999) 57.
[9] C.D. Baertsch, S.L. Soled, E. Iglesia, J. Phys. Chem. B 105 (2001) 1320.
[10] C.D. Baertsch, K.T. Komala, Y.H. Chua, E. Iglesia, J. Catal. 205 (2002) 44.
[11] M. Scheithauer, T.K. Cheung, R.E. Jentoft, R.K. Grasselli, B.C. Gates, H. Knözinger, J. Catal. 180 (1998) 1.
[12] M. Scheithauer, R.K. Grasselli, H. Knözinger, Langmuir 14 (1998) 3019.
[13] S. Kuba, P. Lukinskas, R.K. Grasselli, B.C. Gates, H. Knözinger, J. Catal. 216 (2003) 353.
[14] D.S. Kim, M. Ostromecki, I.E. Wachs, J. Mol. Catal. A 106 (1996) 93.
[15] T. Kim, A. Burrows, C.J. Kiely, I.E. Wachs, J. Catal. 246 (2007) 370.
[16] E.I. Ross-Medgaarden, W.V. Knowles, T. Kim, M.S. Wong, W. Zhou, C.J. Kiely, I.E. Wachs, J. Catal. 256 (2008) 108.
[17] D. Gazzoli, M. Valigi, R. Dragone, A. Marucci, G. Mattei, J. Phys. Chem. B 101 (1997) 11129.
[18] M. Valigi, D. Gazzoli, I. Pettiti, G. Mattei, S. Colonna, S. De Rossi, G. Ferraris, Appl. Catal. A 231 (2002) 159.
[19] G. Ferraris, S. De Rossi, D. Gazzoli, I. Pettiti, M. Valigi, G. Magnacca, C. Morterra, Appl. Catal. A 240 (2003) 119.
[20] T. Onfroy, G. Clet, M. Houalla, J. Phys. Chem. B 109 (2005) 3345.
[21] A. Martínez, G. Prieto, M.A. Arribas, P. Concepción, J.F. Sánchez-Royo, J. Catal. 248 (2007) 288.
[22] V. Lebarbier, G. Clet, M. Houalla, J. Phys. Chem. B 110 (2006) 13905.
[23] R. Thomas, F.P.J.M. Kerkhof, J.A. Moulijn, J. Medema, V.H.J. de Beer, J. Catal. 61 (1980) 559.
[24] T. Yamaguchi, Y. Tanaka, K. Tanabe, J. Catal. 65 (1980) 442.
[25] A. Andreini, J.C. Mol, J. Colloid Interface Sci. 84 (1981) 57.
[26] L.L. Murrell, D.C. Grenoble, C.J. Kim, N.C. Dispenziere Jr., J. Catal. 107 (1987) 463.
[27] S.L. Soled, G.B. McVicker, L.L. Murrell, L.G. Sherman, J.N.C. Dispenziere, S.L. Hsu, D. Waldman, J. Catal. 111 (1988) 286.
[28] W. Grünert, E.S. Shpiro, R. Feldhaus, K. Anders, G.V. Antoshin, K.M. Minachev, J. Catal. 107 (1987) 522.
[29] P. Tittarelli, A. Iannibello, P.L. Villa, J. Solid State Chem. 37 (1981) 5121.
[30] D.C. Vermaire, P.C. van Berge, J. Catal. 116 (1989) 309.
[31] S. Meijers, L.H. Gielgens, V. Ponec, J. Catal. 156 (1995) 147.
[32] L.H. Gielgens, M.G.H. Vankampen, M.M. Broek, R. Vanhardeveld, V. Ponec, J. Catal. 154 (1995) 201.
[33] F. Hilbrig, H.E. Göbel, H. Knözinger, H. Schmelz, B. Lengeler, J. Phys. Chem. 95 (1991) 6973.
[34] S.R.G. Carrazan, C. Martin, G. Solana, V. Rives, Langmuir 17 (2001) 6968.
[35] I. Rodriguez-Ramos, A. Guerrero-Ruiz, N. Homs, P. Ramirez de la Piscina, J.L.G. FierroHoms, J. Mol. Catal. A 95 (1995) 147.
[36] R. Zhang, J. Jagiello, J.F. Hu, Z.Q. Huang, J.A. Schwarz, A. Datye, Appl. Catal. A 84 (1992) 123.
[37] V.M. Benitez, N.S. Figoli, Catal. Commun. 3 (2002) 487.
[38] J. Macht, C.D. Baertsch, M. May-Lozano, S.L. Soled, Y. Wang, E. Iglesia, J. Catal. 227 (2004) 479.
[39] V. Lebarbier, G. Clet, M. Houalla, J. Phys. Chem. B 110 (2006) 22608.
[40] T. Onfroy, V. Lebarbier, G. Clet, M. Houalla, J. Mol. Catal. A 318 (2010) 1.
[41] G. Ghiotti, E. Garrone, C. Morterra, F. Boccuzzi, J. Phys. Chem. 83 (1979) 2863.
[42] T.P. Beebe, P. Gelin, J.T. Yates, Surf. Sci. 148 (1984) 526.
[43] M.I. Zaki, H. Knözinger, Mater. Chem. Phys. 17 (1987) 201.
[44] O. Cairon, T. Chevreau, J.C. Lavalley, J. Chem. Soc. Faraday Trans. 94 (1998) 3039.
[45] K.I. Hadjiivanov, G.N. Vayssilov, Advances in Catalysis, vol. 47, Academic Press Inc., San Diego, 2002, p. 307.
[46] T. Onfroy, G. Clet, M. Houalla, Micropor. Mesopor. Mater. 82 (2005) 99.
[47] S.S. Chan, I.E. Wachs, L.L. Murrell, J. Catal. 90 (1984) 150.
[48] M.A. Vuurman, I.E. Wachs, J. Phys. Chem. 96 (1992) 5008.
[49] T. Onfroy, G. Clet, M. Houalla, J. Phys. Chem. B 109 (2005) 14588.
[50] T. Onfroy, O.V. Manoilova, S.B. Bukallah, D.M. Hercules, G. Clet, M. Houalla, Appl. Catal. A 316 (2007) 184.
[51] E.I. Ross-Medgaarden, I.E. Wachs, J. Phys. Chem. C 111 (2007) 15089.
[52] A. Gervasini, A. Auroux, J. Catal. 131 (1991) 190.
[53] E.R.A. Matulewicz, F.P.J.M. Kerkhof, J.A. Moulijn, H.J. Reitsma, J. Colloid Interface Sci. 77 (1980) 110.
[54] A. Corma, C. Rodellas, V. Fornes, J. Catal. 88 (1984) 374.
[55] C. Morterra, G. Cerrato, G. Meligrana, Langmuir 17 (2001) 7053.
[56] L. Oliviero, A. Vimont, J.C. Lavalley, F. Romero Sarria, M. Gaillard, F. Maugé, Phys. Chem. Chem. Phys. 7 (2005) 1861.
[57] H. Knözinger, C. Ratnasamy, Catal. Rev. Sci. Eng. 17 (1978) 31.
[58] W.S. Millman, M. Crespin, A.C. Cirillo, S. Abdo, W.K. Hall, J. Catal. 60 (1979) 404.
[59] A.M. Turek, I.E. Wachs, E. DeCanio, J. Phys. Chem. 96 (1992) 5000.
[60] N. Vaidyanathan, D.M. Hercules, M. Houalla, Anal. Bioanal. Chem. 373 (2002) 547.
[61] C. Morterra, G. Magnacca, Catal. Today 27 (1996) 497.
[62] A.L. Diaz, M.E. Bussell, J. Phys. Chem. 97 (1993) 470.
[63] V.M. Benitez, C.A. Querini, N.S. Figoli, R.A. Comelli, Appl. Catal. A 178 (1999) 205.
[64] T. Onfroy, G. Clet, S.B. Bukallah, T. Visser, M. Houalla, Appl. Catal. A 298 (2006) 80.